*International Journal of Applied Mathematics and Theoretical Physics*
2025, Vol. 11, No. 3, pp. 36-43
https://doi.org/10.11648/j.ijamtp.20251103.11

Research Article

# Examining the Angular Distribution of Deuteron Scattering from $^6$Li and $^9$Be in the Elastic Channel

**Raymond Chivirter Abenga*, Gertrude Ashia Bijimi**

Department of Pure and Applied Physics, Veritas University Abuja, Abuja, Nigeria

## Abstract

The theoretical analyses of the elastic scattering of deuteron from $^6$Li, and $^9$Be were performed in the optical model (OM) framework. The double-folding model with a density-dependent M3Y-type effective interaction was used to derive both the real and the imaginary components of the optical potential. The derived nuclear optical potentials were subsequently employed in the OM formalism to analyse the angular distribution data of deuteron scattering from $^6$Li, and $^9$Be at different incident energies. The calculated differential cross-sections were compared with experimental data across multiple incident energies. The results demonstrate that the derived potentials accurately reproduce experimental observables, confirming the reliability of the double-folding model and the OM for modelling light-ion scattering. These findings also underscore the applicability of the M3Y-type interaction in describing short-range nuclear interactions in light nuclei.

## Keywords

Angular Distribution, Elastic Scattering, Folding Potential, Pseudo-Potential, M3Y-Type Interaction, S-Matrix

## 1. Introduction

The intricate many-body nature of nucleus-nucleus interactions remains a topic that is not yet fully understood. Continuous improvements are being made to theoretical models and techniques to tackle this complex problem [1]. A key approach to advancing the understanding of the complex many-body problem of the nucleus-nucleus interaction involves a detailed analysis of experimental results within theoretical frameworks. Specifically, analysing heavy-ion data through models like the optical model, coupled channels, and coupled reaction channels yields valuable insights into the general features of nucleus-nucleus interactions, including their energy dependence and links to nuclear structure [2].

Heavy-Ion (HI) scattering is marked by strong absorption, which occurs when part of the incoming wave is diverted from the elastic scattering path into other, non-elastic channels [3, 4]. As a result, the optical potential used to describe HI interactions always includes an imaginary component. The real component accounts for elastic scattering, while the imaginary part represents absorption and the loss of flux from the elastic channel [2, 5]. Because of this strong absorption, only peripheral collision paths are useful in probing the real part of the nucleus-nucleus interaction, particularly near the nuclear surface [4]. The radius where this surface interaction becomes significant is identified as the strong absorption radius.

Therefore, it has become particularly important to develop theoretical tools to investigate the nuclear structures and nuclear reactions of HI scattering. In recent times, the mass-dependent interactions dubbed the M3Y-type interac-

*Corresponding author: abengar@veritas.edu.ng (Raymond Chivirter Abenga)

**Received:** 9 June 2025; **Accepted:** 2 July 2025; **Published:** 7 August 2025

Copyright: © The Author(s), 2025. Published by Science Publishing Group. This is an **Open Access** article, distributed under the terms of the Creative Commons Attribution 4.0 License (http://creativecommons.org/licenses/by/4.0/), which permits unrestricted use, distribution and reproduction in any medium, provided the original work is properly cited.

tions, derived using the lowest order constrained variational approach, were constructed [6-9]. The interactions were derived using nuclei of mass number $A = 16, 24, 40$, and 90 [8]. Although the strengths of the interactions showed mass dependence, it was recommended that they could be used in the study of nuclear structure and reactions for all nuclei.

The primary objective of this study is to derive optical potential parameters for the elastic scattering of deuteron from $^{6}Li$ and $^{9}Be$ nuclear system. The double folding model (DFM) was applied, employing the density-dependent version of the M3Y-type interaction to derive the strengths of the optical potential. The analyses of the differential cross-sections were done using a phenomenological optical model (OM) approach.

## 2. Materials and Methods

To construct the nuclear optical potential, the double-folding model was used. The double-folding model convolves the effective NN interaction with the nuclear density distributions of the projectile and target [4]:

$$V_F(r) = \iint \rho_p(\mathbf{r}_p)\rho_t(\mathbf{r}_t)V_{pt}(\mathbf{r}_{tp})dr_p dr_t \quad (1)$$

here $\rho_p$ and $\rho_t$ are the density distributions of the projectile and target nuclei, and $\mathbf{r}_{tp} = r_t - r_p$ and the term $V_{pt}$ is the effective M3Y-type density-dependent interaction [2, 10, 11]. The nuclear densities are modelled using the two-parameter Fermi (2pF) distribution [12, 13]:

$$\rho(r) = \rho_0\left[1 + \exp\left(\frac{r-c}{a}\right)\right]^{-1} \quad (2)$$

here, $\rho_0$, c, and $a$ are the central density, the half-density radius, and the diffuseness parameter, respectively. The 2pF function was parametrised in the manner prescribed by [14], for both the incident and the target nuclei. The double folding model calculations were done using the folding model code of the Nuclear Reaction Video (NRV) [15].

The double-folded potential naturally represents the real part of the optical potential. To account for the imaginary part—which captures absorption into non-elastic channels—a similar folding approach was applied but with a different renormalization factor to obtain the nuclear optical potential in the form [11]:

$$U(r) = (N_r + iN_i)V_F(r) + V_{Coul}(r) \quad (3)$$

where $N_{r(i)}$ are the real and imaginary renormalization factors for the folded potential and $V_{Coul}(r)$ is the Coulomb potential. These renormalization constants are adjusted to achieve optimal agreement with experimental data.

The optical potential formulation of Equation (3) was modified to include potential geometrical parameters. These geometrical parameters were assumed to have the Woods-Saxon form factor. The nuclear part of the OP of Equation (3) was modified to include the geometrical parameters in the form;

$$V_N = -[V_0 f(r, R_v, a_v) + iW_0 f(r, R_w, a_w)] \quad (4)$$

where $V_0$ and $W_0$ are the strengths of the real and imaginary folded potentials, respectively, and $f(r, R_i, a_i)$ is the introduced Woods-Saxon form factor with $i = v, w$. The geometrical form factor introduced in Equation (4) is defined by [16];

$$f(r, R_i, a_i) = \left(1 + \exp\left[\frac{r-R_i}{a_i}\right]\right)^{-1} \quad (5)$$

where $R_i$ and $a_i$ are the half-value radius and the diffuseness parameters, which describe the decreasing rate of the optical potential. The radius parameters were defined by [14];

$$R_i = \left[r_i\left(A_p^{\frac{1}{3}} + A_t^{\frac{1}{3}}\right)\right] \quad (6)$$

while the diffuseness parameter was defined by:

$$a_i = 0.734 - \frac{150}{Z_t^2 + 500} \quad (7)$$

where $A_{p(t)}$ are the mass numbers of the projectile and target nuclei, and $Z_t$ is the atomic number of the target.

The introduced geometrical parameters were deduced by fitting the elastic scattering data using the double folding potential by minimising the $\chi^2$ value in the OM code. The best value of $\chi^2$ was defined by [17, 18]:

$$\chi^2 = \frac{1}{N}\sum_{i=1}^{N}\left[\frac{\sigma_{cal}(\theta_i) - \sigma_{exp}(\theta_i)}{\Delta\sigma_{exp}(\theta_i)}\right]^2 \quad (8)$$

where $\sigma_{cal}(\theta_i)$ and $\sigma_{exp}(\theta_i)$ are, respectively, the calculated and experimental values of the elastic scattering differential cross-section at $\theta_i$ and $\Delta\sigma_{exp}(\theta_i)$ is the corresponding experimental error. At the same time, N is the number of data points.

## 3. Results

The analyses of elastic scattering of $d + {}^{6}Li$ and $d + {}^{9}Be$ were performed using the parameterised M3Y-type interaction in the double-folding model framework. The strengths of the folded potentials were evaluated. The calculated reaction cross-sections were consistent with experimentally measured ones and those obtained using other theoretical methods [19-22]. The deduced best-fit parameters of the double-folding calculations are presented in Table 1.

***Table 1.*** *Best-fit parameters deduced from the double folding calculations of elastic scattering of deuteron from* $^6Li$ *and* $^9Be$.

| Target | $E_{lab}$ (MeV) | $N_r$ | $N_i$ | $\sigma_r$ (mb) | $\sigma_{tot}$ (mb) |
|---|---|---|---|---|---|
| $^6$Li | 25 | 1.50 | 0.72 | 825.97 | 1480.33 |
| | 171 | 1.80 | 0.90 | 437.63 | 850.07 |
| $^9$Be | 15.8 | 1.20 | 0.50 | 960.99 | 1692.04 |
| | 27.7 | 1.25 | 0.55 | 848.97 | 1564.81 |

The sensitivity of the strengths of the folded potential was carried out by varying $N_r$ and $N_i$ around best-fit values to the experimental data. The results showed that the differential cross-sections were more sensitive to $N_r$ than the $N_i$. particularly, the variation of $N_i$ values only impacted the magnitude of the absorption potential. The real renormalisation factors in Table 1 show that the strengths of real potentials were underestimated, hence the tuning of the renormalization factors to values greater than unity. On the other hand, the imaginary potentials had factors less than unity, suggesting their strengths were overestimated and thus required reduction. In conclusion, the derived folded potentials were found appropriate for the studies of nuclear reactions, as physical observables of the reactions were well reproduced.

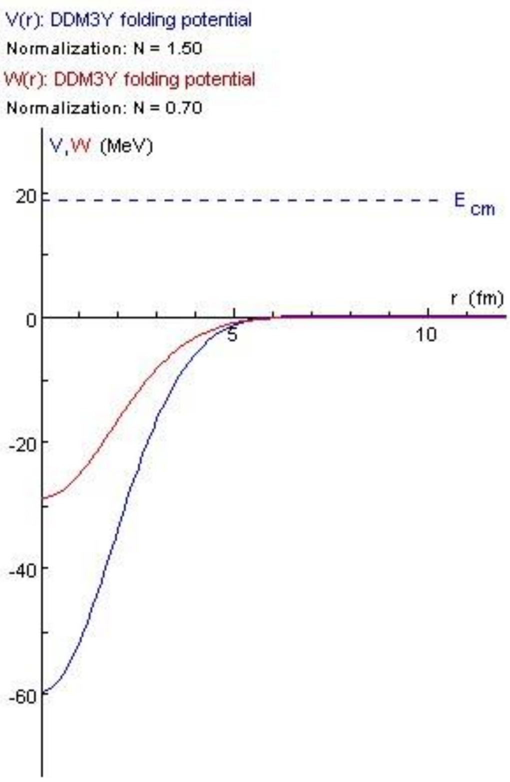


***Figure 1.*** *Radial shape of the real and imaginary components of the double-folded optical potential of* $d + {}^6Li$ *elastic scattering at* $E_{lab} = 25\ MeV$.

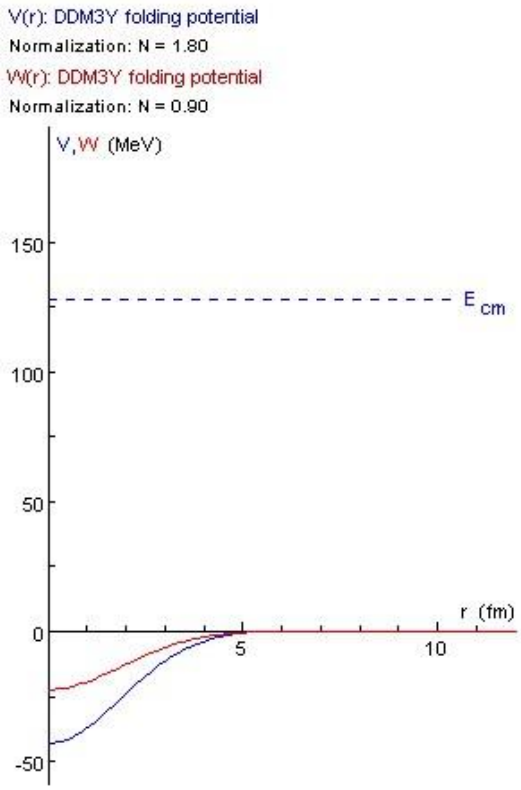


***Figure 2.*** *Radial shape of the real and imaginary components of the double-folded optical potential of* $d + {}^6Li$ *elastic scattering at* $E_{lab} = 171\ MeV$.

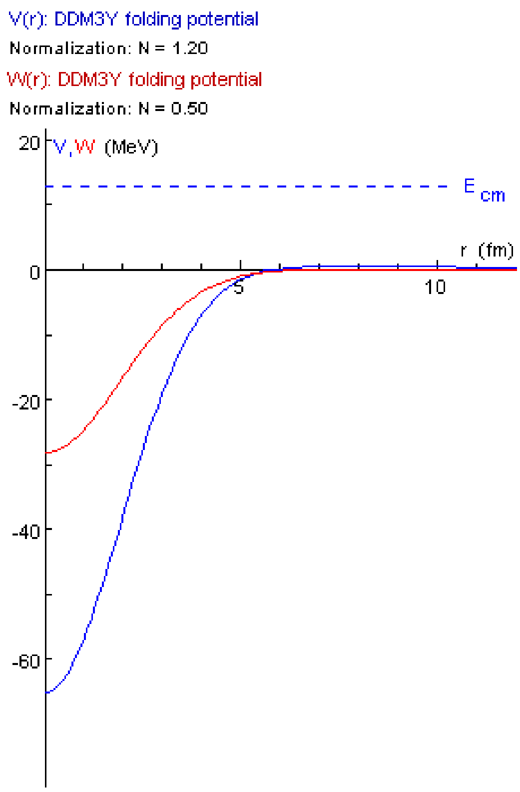


***Figure 3.*** *Radial shape of the real and imaginary components of the double-folded optical potential of* $d + {}^6Li$ *elastic scattering at* $E_{lab} = 15.8\ MeV$.

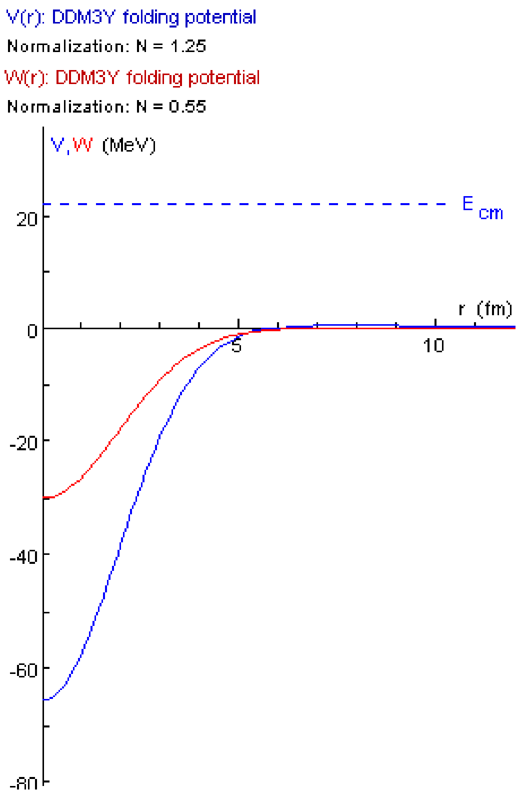


***Figure 4.*** *Radial shape of the real and imaginary components of the double-folded optical potential of* $d + {}^{6}Li$ *elastic scattering at* $E_{lab} = 27.7\ MeV$.

The depths of the folded potentials were obtained, and the plots of the depths of the folded potentials to the radial distance (r) are given in Figures 1-4. The depths of the folded potentials assumed the Woods-Saxon form and were found to be attractive and short-ranged within short internuclear distances of $0 \leq r \leq 5.5$ fm at all energies. The blue curves of Figures 1-4 represent the results of the real part of the folded potential, while the red curves denote the imaginary parts of the folded potentials. The real parts of the folded optical potentials were found to be deeper than the imaginary part at all incident energies. This observation is a manifestation of the larger $N_r$ values that were needed to optimise the fit of the scattering data.

It was observed that the $\chi^2$ value obtained for the 27.7 MeV scattering data of the deuteron on $^{9}Be$ was exceptionally large, implying a poor fit quality. This large value of $\chi^2$ could likely be attributed to limitations in the OM at this energy or unaccounted contributions from other reaction mechanisms. The geometrical parameters of these interactions were derived, and the results are presented in Table 2. The extracted radii $R_{v(w)}$ indicates that the nuclear surface extends slightly beyond the nominal strong absorption radius. This indicates that the elastic scattering of deuteron from $^{6}Li$, and $^{9}Be$ predominantly probes the surface region of $^{6}Li$, and $^{9}Be$. On the other hand, the larger values of $a_w$ implies a stronger surface absorption effect, which is consistent with significant coupling to non-elastic channels in these reactions.

***Table 2.*** *Best-fit geometrical parameters of the real and imaginary parts of the optical potential for* $d + {}^{6}Li$ *and* $d + {}^{9}Be$ *elastic scattering at different incident energies.* $\chi^2$ *values reflect the quality of the fit between theoretical and experimental cross-sections.*

| Target | $E_{lab}$ (MeV) | $V_r$ (MeV) | $R_v$ (fm) | $a_v$ (fm) | $W_i$ (MeV) | $R_w$ (fm) | $a_w$ (fm) | $\chi^2$ |
|---|---|---|---|---|---|---|---|---|
| $^{6}Li$ | 25 | 66.14 | 0.87 | 0.76 | 31.41 | 0.75 | 0.81 | 16.17 |
| | 171 | 50.49 | 0.65 | 0.75 | 16.63 | 0.78 | 1.11 | 2.97 |
| $^{9}Be$ | 15.8 | 63.30 | 0.88 | 0.83 | 33.07 | 0.75 | 0.81 | 4.59 |
| | 27.7 | 66.00 | 0.79 | 0.89 | 30.00 | 1.01 | 0.43 | 5756.92 |

The differential cross-sections of deuteron scattering from $^{6}Li$ and $^{9}Be$ were measured using the derived folded potential in the elastic channel. The plots of differential cross sections relative to the angles in the centre of mass are shown in Figures 5-8. The solid line in these figures represents the result of the theoretical calculations, while the solid dots correspond to the experimental data. The fits between the angular distributions of the theoretical calculations and the experimental data were well reproduced at all incident energies. However, small deviations were observed in the backward angles. The deviation observed between the theoretical predictions and experimental data at backward angles can be attributed to additional reaction mechanisms like breakup or nucleon transfer that were not accounted for by the present optical model. The observed minimum in the $d + {}^{6}Li$ scattering data at 25 MeV was not peculiar to this work; it was also observed when phenomenological potentials were used [23].

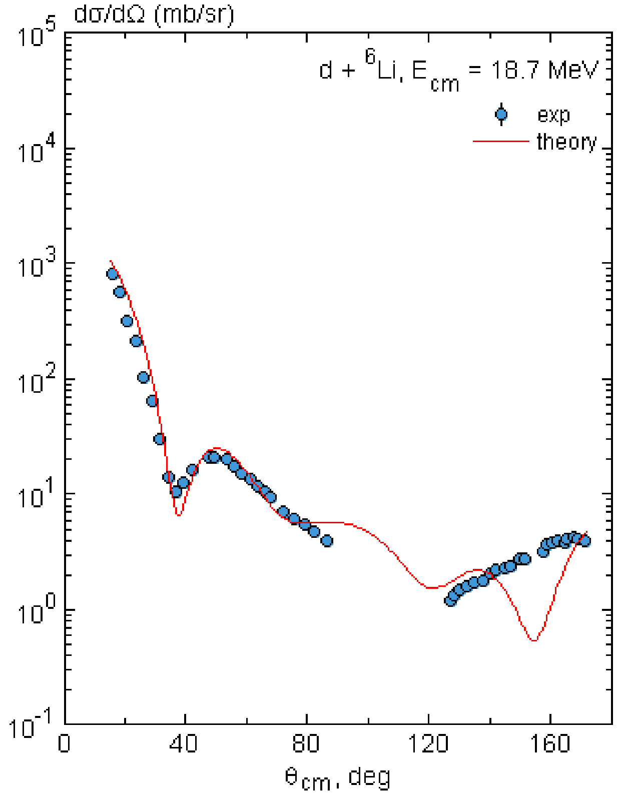


***Figure 5.*** *Angular distributions of* $d + {}^{6}Li$ *elastic scattering at* $E_{lab} = 25\ MeV$.

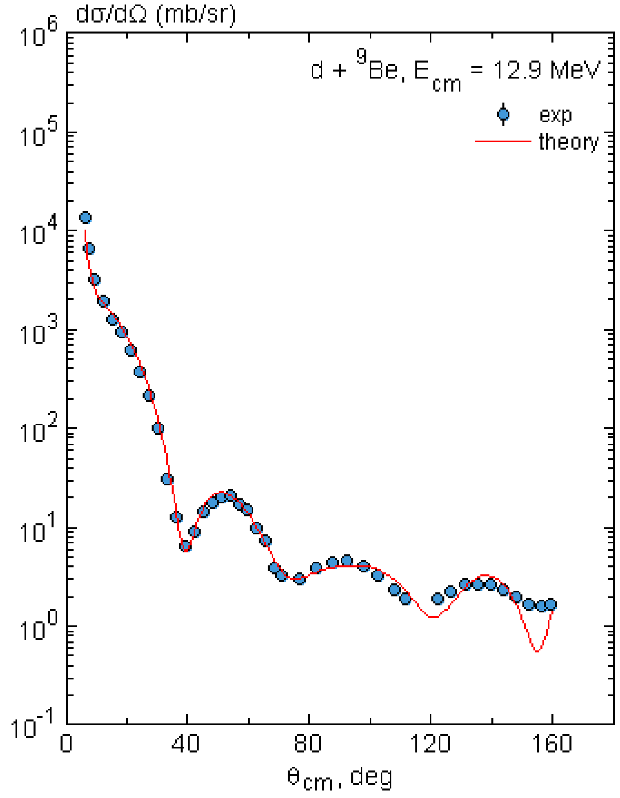


***Figure 7.*** *Angular distribution of* $d + {}^{9}Be$ *elastic scattering at* $E_{lab} = 15.8\ MeV$.

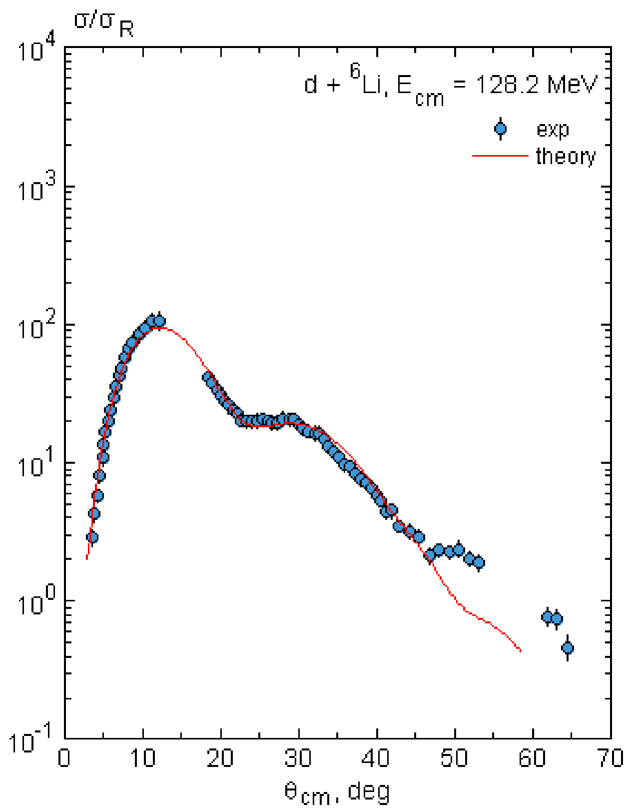


***Figure 6.*** *Angular distributions of* $d + {}^{6}Li$ *elastic scattering at* $E_{lab} = 171\ MeV$.

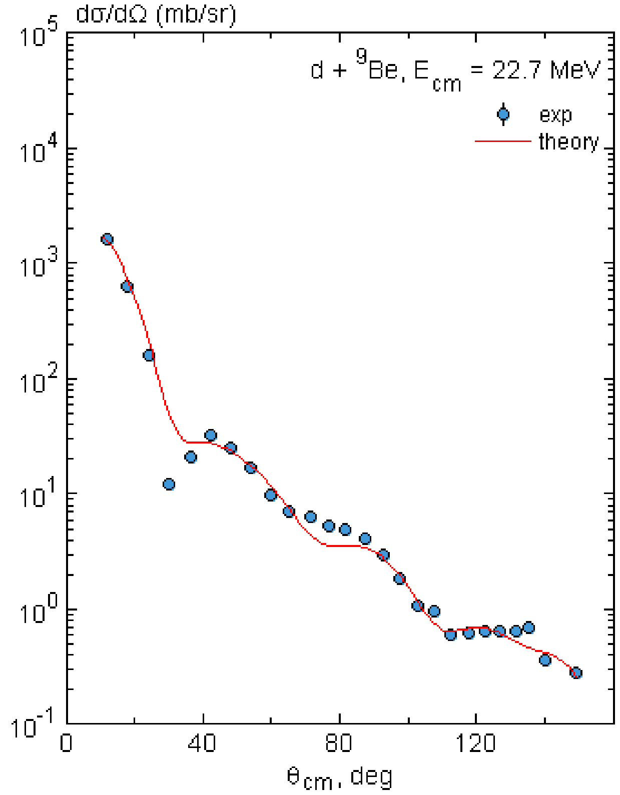


***Figure 8.*** *Angular distribution of* $d + {}^{9}Be$ *elastic scattering at* $E_{lab} = 27.7\ MeV$.

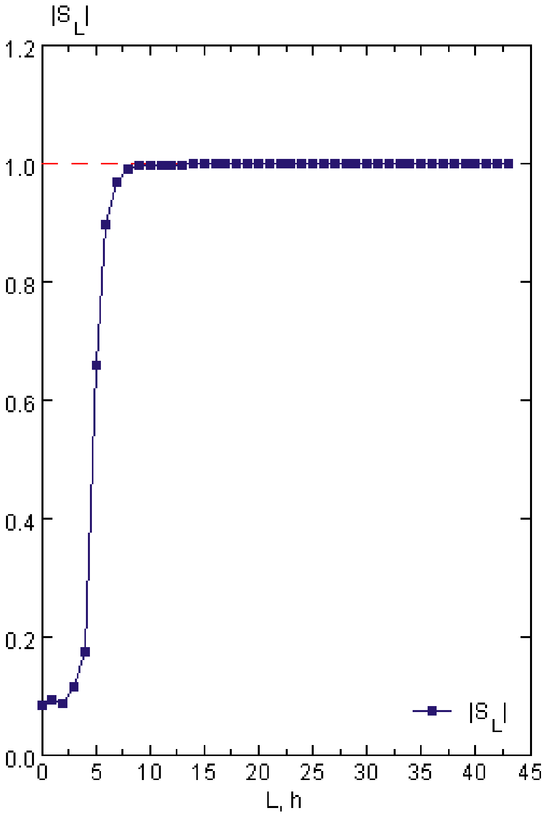


***Figure 9.*** *Modulus of the elastic S-matrix as a function of total orbital angular momentum of* $d + {}^{6}Li$ *at* $E_{lab} = 25\ MeV$.

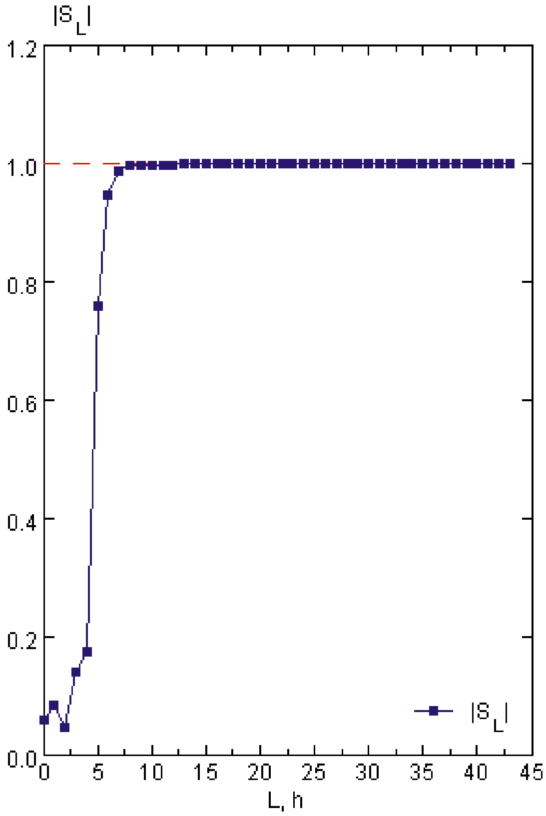


***Figure 11.*** *Modulus of the elastic S-matrix as a function of total orbital angular momentum of* $d + {}^{9}Be$ *at* $E_{lab} = 15.8\ MeV$.

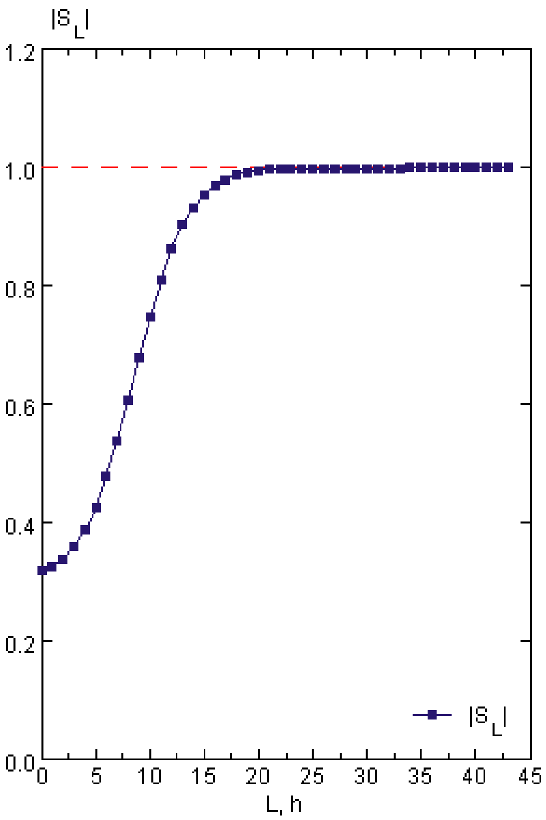


***Figure 10.*** *Modulus of the elastic S-matrix as a function of total orbital angular momentum of* $d + {}^{6}Li$ *at* $E_{lab} = 171\ MeV$.

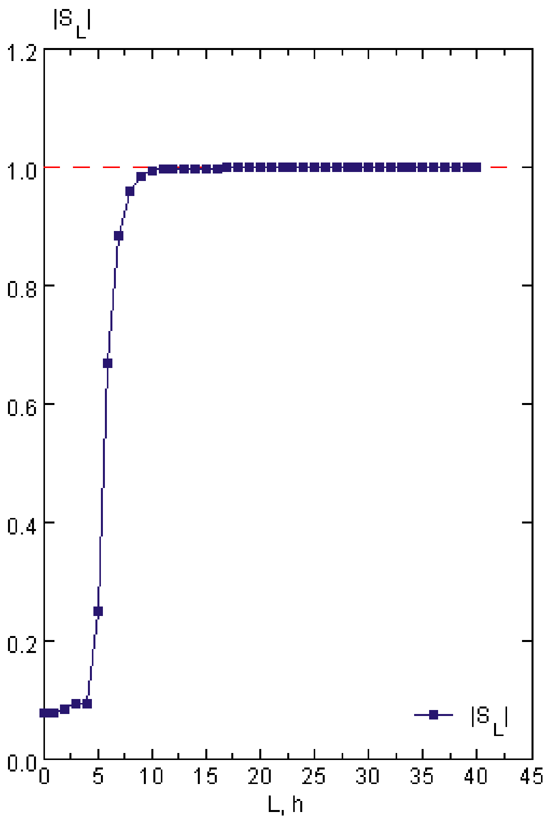


***Figure 12.*** *Modulus of the elastic S-matrix as a function of total orbital angular momentum of* $d + {}^{9}Be$ *at* $E_{lab} = 27.7\ MeV$.

To analyse the absorption effect of the formulated nuclear potential, the moduli of the S-matrix were obtained. The plots of the moduli of the S-matrix elements to the angular momenta are shown in Figures 9-12. The plots of the moduli of $S_L$ revealed that the nuclear potential made a significant contribution to the interactions within small impact parameters between $0 \le L \le 10$. Beyond this range, the magnitude of $S_L$ was found to be maximum, i.e., $(|S_L| = 1)$. In the case of the $171$ MeV scattering data, the $|S_L|$ values ranged from $0.3 \le |S_L| \le 1$ in the angular region of $0 \le L \le 20$. From the plot of the S-matrix element, it was further seen that absorption effects were present as seen in the range of values of L, for which $|S_L| \le 1$, however, no region of complete absorption was observed.

## 4. Conclusion

This study investigated the elastic scattering of deuterons from $^{6}Li$, and $^{9}Be$ using a double-folding optical model potential derived from the density-dependent M3Y-type interaction. The derived optical potentials successfully reproduced the measured angular distributions and reaction cross-sections across a range of incident energies. Renormalization factors indicated that the real parts of the potentials were generally underestimated, while the imaginary parts were overestimated—a trend consistent with theoretical expectations in light-ion scattering. The folded potentials exhibited Woods-Saxon-like radial behaviour, confirming their short-range, attractive nature. Additionally, the S-matrix analyses revealed realistic absorption behaviour at small impact parameters, with no dominant region of strong absorption. The overall agreement with experimental data validates the use of the M3Y-type interaction and supports its further application in modelling nuclear reaction studies. While the present optical model analysis reproduces the overall angular distributions reasonably well, its limitations must be acknowledged. The model does not explicitly account for coupling reaction mechanisms in other non-elastic channels, which likely contributes to the discrepancies at backward angles and the high $\chi^2$ values for certain energy sets. Future studies will incorporate coupled-channel calculations to address these shortcomings.

## Abbreviations

| | |
|---|---|
| DFM | Double-Folding Model |
| HI | Heavy-Ion |
| M3Y | Michigan Three Yukawa |
| NRV | Nuclear Reaction Video |
| OM | Optical Model |

## Conflicts of Interest

The authors declare no conflicts of interest.

## References


[1] H. Amer, Z. M. M. Mahmoud, and M. N. El-hammamy, "Analysis of $^{9}$Be + $^{28}$Si elastic scattering system using different optical potentials," *Chinese J. Phys.*, vol. 92, pp. 195-210, 2024, https://doi.org/10.1016/j.cjph.2024.01.024

[2] R. C. Abenga, Y. Y. Ibrahim, I. D. Adamu, and L. Ibrahim, "Strong Absorption and the Double Folding Potential Using B3Y-Fetal Interaction," *Caliphate J. Sci. Technol.*, vol. 6, no. 3, pp. 323-332, 2024.

[3] G. R. Satchler, *Direct Nuclear Reactions*. Oxford University Press, 1983.

[4] G. R. Satchler and W. G. Love, "Folding model potentials from realistic interactions for heavy-ion scattering," *Phys. Reports (Review Sect. Phys. Lett.*, vol. 55, no. 3, pp. 183-254, 1979, https://doi.org/10.1016/0370-1573(79)90081-4

[5] R. C. Abenga, Y. Y. Ibrahim, and I. D. Adamu, "The Folding Potential of Elastically Scattered d+ $^{24}$Mg Employing B3Y-Fetal Interaction within the Double Folding Model Framework," *UMYU Sci.*, vol. 3, no. 3, pp. 239-250, 2024.

[6] I. Ochala, J. O. Fiase, and E. Anthony, "Computation of Nuclear Binding Energy and Incompressibility with a New M3Y-Type Effective Interaction," *Int. Res. J. Pure Appl. Phys.*, vol. 5, no. 3, pp. 5-13, 2017.

[7] R. C. Abenga, J. O. Fiase, and G. J. Ibeh, "Optical model analysis of α+ $^{40}$Ca at $E_{lab}$ = 104 and 141.7 MeV using a mass-dependent M3Y-type effective interaction," *Niger. Ann. Pure Appl. Sci.*, vol. 3, no. 2, pp. 252-260, 2020.

[8] J. O. Fiase, K. R. S. Devan, and A. Hosaka, "Mass dependence of M3Y-type interactions and the effects of tensor correlations," *Phys. Rev. C - Nucl. Phys.*, vol. 66, no. 1, pp. 014004-10, 2002, https://doi.org/10.1103/PhysRevC.66.014004

[9] I. Ochala, D. Terver, and J. O. Fiase, "A study of $^{12}$C+$^{12}$C nuclear reaction using a new M3Y-type eff ective interaction," pp. 133-142, 2020, https://doi.org/10.29328/journal.ijpra.1001031

[10] R. C. Abenga, Y. I. Yahaya, and I. D. Adamu, "Double Folding Potential of Deuteron Elastic Scattering on Target Nuclei in the Mass Range of 50≤ A ≤ 208 Using a Mass-Dependent Effective Interaction," *Bayero J. Phys. Math. Sci.*, vol. 01, no. 13, pp. 1-14, 2021.

[11] R. C. Abenga, Y. Y. Ibrahim, and I. D. Adamu, "Double Folding Potential and the Deuteron-Nucleus Inelastic Scattering in the Optical Model Framework," *Open Access Libr. J.*, vol. 10, pp. 1-16, 2023, https://doi.org/10.4236/oalib.1109550

[12] G. R. Satchler, "A simple effective interaction for peripheral heavy-ion collisions at intermediate energies," *Nucl. Phys. A*, vol. 579, pp. 241-255, 1994.

[13] A. L. El-Attar, M. E. Farid, and M. G. El-Aref, "Optical Model Analyses of Deuteron Inelastic Scattering," in *9th International Conference for Nuclear Sciences and Applications, Sharm Al Sheikh (Egypt)*, Egypt, 2008, p. 1239.

[14] S. D. Olorunfunmi and A. S. Olatinwo, "Analysis of Elastic Scattering Cross Sections of $^{16}O$ on $^{27}Al$ and $^{154}Sm$ Using the Semi-Microscopic Double Folding Model," *Ife J. Sci.*, vol. 25, no. 2, pp. 239-250, 2023.

[15] V. Zagrebaev, A. Denikin, and A. Alekseev, "Optical model of elastic scattering, Nuclear Reaction Video Project". http://nrv.jinr.ru/nrv/webnrv/elastic_scattering/els1.htm 2000

[16] H. An and C. Cai, "Global deuteron optical model potential for the energy range up to 183 MeV," *Phys. Rev. C - Nucl. Phys.*, vol. 73, no. 5, pp. 054605-9, 2006, https://doi.org/10.1103/PhysRevC.73.054605

[17] M. E. Farid, L. Alsagheer, W. R. Alharbi, and A. A. Ibraheem, "Analysis of Deuteron Elastic Scattering in the Framework of the Double Folding Optical Potential Model," *Life Sci. J.*, vol. 11, no. 5, pp. 208-216, 2014, http://dx.doi.org/110.21043/equilibrium.v3i2.1268

[18] A. A. Ibraheem, A. Branch, M. E. Farid, and E. F. Elshamy, "Comprehensive Examination of the Elastic Scattering Angular Distributions of $^{10}C$+$^{4}He$, $^{27}Al$, $^{58}Ni$ and $^{208}Pb$ Using Various Potentials," *Rev. Mex. Defisica*, vol. 69, no. June, pp. 1-13, 2023.

[19] A. A. Ibraheem, "Analysis of Deuteron-Nucleus Scattering Using Sao Paulo Potential," *Brazilian J. Phys.*, vol. 46, no. 6, pp. 746-753, 2016, https://doi.org/10.1007/s13538-016-0453-0

[20] A. Korff, P. Haefner, C. Bäumer, A. M. van den Berg, N. Blasi, B. Davids, D. De Frenne, R. de Leo, D. Frekers, E. W. Grewe, M. N. Harakeh, F. Hofmann, M. Hunyadi, E. Jacobs, B. C. Junk, A. Negret, P. von Neumann-Cosel, L. Popescu, S. Rakers, A. Richter, and H. J. Wörtche, "Deuteron Elastic and Inelastic Scattering at Intermediate Energies from Nuclei in the Mass Range $6 \le A \le 116$," *Phys. Rev. C*, vol. 70, no. 6, pp. 0676011-0676014, 2004, https://doi.org/10.1103/PhysRevC.70.067601

[21] A. A. Cowley, G. Heymann, R. L. Keizer, and M. J. Scott, "Elastic and inelastic scattering of 15.8 MeV deuterons," *Nucl. Phys.*, vol. 86, no. 2, pp. 363-377, 1966, https://doi.org/10.1016/0029-5582(66)90544-X

[22] R. J. Slobodrian, "Scattering of 27.7 MeV Deuterons on Beryllium and Boron," *Nucl. Phys.*, vol. 32, no. May 1961, pp. 684-694, 1962.

[23] N. Burtebayev, S. V. Artemov, B. A. Duisebayev, Z. K. Kerimkulov, S. B. Kuranov, and S. B. Sakuta, "Deuteron scattering on $^{6}Li$ at an energy of 25 MeV," *Phys. At. Nucl.*, vol. 73, no. 5, pp. 746-756, May 2010, https://doi.org/10.1134/s1063778810050030